AIAA JOURNAL
Vol. 44, No. 6, June 2006

Improving the Predictive Capability of Turbulence Models Using Evidence Theory

Svetlana V. Poroseva,* M. Yousuff Hussaini,† and Stephen L. Woodruff‡
Florida State University, Tallahassee, Florida 32306-4120

When turbulence models are used in the simulation of a flow for which experimental results do not exist, there is, as yet, no reliable procedure for choosing a model or for quantifying the uncertainty of the results. In fact, even if experimental data are available, there appears to be no general procedure to quantify uncertainty in simulations. The present study explores the potential of employing the Dempster–Shafer theory of evidence to address these issues and proposes an approach to quantify uncertainty in turbulent flow simulations. The approach is tested using a subsonic flow around the RAE 2822 airfoil.

Nomenclature

a_{ij}, b_{ij}, c_{ij}	=	matrix elements
c	=	airfoil chord
k	=	turbulent kinetic energy
M	=	Mach number
m	=	basic probability assignment
N	=	number of experimental data in the y direction at a given x/c position
n	=	number of experimental data in a given deviation interval
P	=	proposition probability
U	=	mean velocity
$\boldsymbol{U}$	=	set of all possible mean velocity values
U_e	=	experimental mean velocity or error boundaries, if an experimental error range is available
U_m	=	calculated velocity
U_p	=	predicted velocity
U_∞	=	freestream velocity
x	=	direction along the airfoil chord
y	=	direction normal to the airfoil surface
α	=	angle of attack
ΔDev	=	deviation step
ε	=	dissipation rate
ω	=	ε/k

I. Introduction

COMPUTATIONAL fluid dynamics (CFD) simulations have become a primary tool for the prediction of flows of scientific and engineering interest. To draw meaningful conclusions from the results of such simulations, information about their accuracy is necessary. In the late 1980s this topic began to receive attention. In Ref. 1, earlier discussions on the subject are summarized and general guidelines for verification and validation of CFD simulations are provided.

Turbulent flow simulations are among the most challenging problems in CFD. Results of turbulent simulations reflect uncertainties due to the deficiency of a turbulence model to describe correctly the flow physics, uncertainties in boundary conditions, initial conditions, and model parameters, and errors due to discretization and incomplete convergence.[1–5] Typically, one assumes that the higher the model fidelity, the grid resolution, and the formal order of accuracy of a numerical scheme, the more credible are the results of simulations. However, the critical question is how accurate are the results of computations based on the model rather than just how physically correct the model itself is. Moreover, to evaluate the validity of assumptions underlying a turbulence model, one has to carry out computations and compare the computational results with the experimental data or the results of direct numerical simulations. Similar arguments hold for other uncertainty sources as well. In other words, the sum of contributions from all uncertainty sources (or the total uncertainty) in simulations is of prime concern. To find an appropriate measure to quantify the total uncertainty in a simulation is one of the objectives of our research.

There are many ways of describing the total uncertainty in simulations. One way would be to identify and describe all sources of uncertainty. (A thorough discussion on identification of uncertainty sources in simulations may be found in Ref. 5 and the references therein.) The attractiveness of this idea is clear. If one could identify and describe all uncertainty sources, contributions from at least some of them could be eliminated or reduced, thereby making simulations more credible. However, the identification of all uncertainty sources in real-flow simulations could be an impossible task. Even if some sources of uncertainty are identified, there still remains the problem of describing their contributions because these sources might affect one another in complicated and generally unknown ways. For instance, decreasing the contribution from one source can increase uncertainty from other sources, resulting in increased total uncertainty. Turbulence models are an example of such an influence on simulation accuracy: a more physically realistic turbulence model is usually also a more complex one (more model parameters, more equations), and as a result, the implementation of a more realistic model can in fact decrease the simulation accuracy.[1] There is a hope that interactions among some uncertainty sources established in benchmark problems will also hold in general cases. Studies should be conducted to answer these and other questions related to individual quantification of various uncertainty sources before this approach could become routine for engineers.

In the present study, we focus on describing the total uncertainty in simulations without distinguishing between contributions from different sources. The total uncertainty in flow simulations has features of both aleatory and epistemic uncertainties currently recognized. Aleatory uncertainty is due to stochastic influences, for example, random noise, and cannot be reduced. Epistemic uncertainty is subjective and originates from incomplete knowledge at any stage of modeling or simulation. Increasing one's knowledge reduces epistemic uncertainty. One needs to be aware of the distinction between uncertainty and error. The latter is defined as

Presented as Paper 2005-1096 at the AIAA 43rd Aerospace Sciences Meeting, Reno, NV, 10–13 January 2005; received 25 January 2005; revision received 27 September 2005; accepted for publication 12 October 2005.

*Research Associate, School of Computational Science and Information Technology. Member AIAA.
†Sir James Lighthill Professor of Mathematics and Computational Science and Engineering.
‡Assistant Scholar Scientist, Center for Advanced Power Systems.

"a recognizable deficiency in any phase or activity of modeling and simulation that is not due to lack of knowledge."[1] In practice, however, when the total uncertainty is of prime concern, separation between uncertainties and errors might not be useful. If an error is not acknowledged, then it falls into a category of uncertainty due to the lack of knowledge. When we do not know how to eliminate the influence of an acknowledged error, then it also contributes in the total simulation uncertainty as uncertainty due to lack of knowledge.

There are several mathematical theories[6] that describe uncertainty and provide its measures: probability theory, possibility theory, and evidence theory. Probability theory, for instance, is better suited to describe aleatory uncertainty. Possibility theory[7] was developed mainly to describe epistemic uncertainty. An extensive literature exists[6,8–10] in which various uncertainty theories are compared, their relations are established, and their advantages and limitations are discussed. Evidence theory is among the well-established theories that can handle both types of uncertainty and does not require their separation. In fact, probability and possibility theories are branches of evidence theory. The theory works with limited information and new data can be incorporated as they become available. These features make evidence theory attractive for application to CFD problems.

In the present study, we explore the potential of the Dempster–Shafer theory of evidence (see Ref. 9) to quantify uncertainty in turbulent flow simulations and develop a mathematically reliable procedure to quantify and possibly reduce the uncertainty of predictive simulations in situations wherein no reference data (experimental or direct numerical simulation data) are available.[1] A key element of the present approach is Dempster's rule, which is one of the basic tools of evidence theory (see Ref. 9). Its valid application requires that 1) the sources of information are independent and 2) they do not strictly contradict one another. These requirements provoked discussion later[11,12] and resulted in various modifications of the rule, for example, as in Refs. 13 and 14. The present work employs the evidence theory formalism in its original form. Requirements of Dempster's rule and how to meet them in the specific engineering problem considered in this paper are discussed in the following sections.

II. Evidence Theory Terminology and Tools

In this paper, we follow the axiomatic approach of evidence theory given by Shafer in Ref. 9. A comprehensive exposition of the foundations of evidence theory may also be found in Refs. 12–16. In the interest of saving space, a brief description of the basic concepts of the theory is provided here for the sake of completeness.

Evidence theory provides two basic tools for quantifying uncertainty in simulations and improving predictions: 1) a tool for representing the degree of belief (confidence) that may be attributed to a given proposition on the basis of given evidence and 2) a tool for combining evidence from different sources (Dempster's rule). Let U be a quantity and $\boldsymbol{U}$ the finite set of its possible values. Then, propositions can be of the following form: the true value of U is in A, where A is a subset of $\boldsymbol{U}$. Whenever A is interpreted as a proposition, its complement $\bar{A}$ (the set of all elements of $\boldsymbol{U}$ not in A) must be interpreted as the proposition's negation. The set of all subsets of $\boldsymbol{U}$, the power set, includes the empty set $\varnothing$ (corresponding to a necessarily false proposition because the true value cannot lie in $\varnothing$) and the entire set $\boldsymbol{U}$ (corresponding to a necessarily true proposition because the true value is assumed to be in $\boldsymbol{U}$).

In evidence theory, the impact of evidence on our belief in different propositions is described by three related functions: the basic probability assignment function m, the belief function (Bel), and the plausibility function (Pl). The basic probability assignment function assigns a number $m(A)$ to each subset A of $\boldsymbol{U}$ such that $m(\varnothing)=0$ for the empty set $\varnothing$, and the sum of basic probability assignments (BPAs) for all subsets A of $\boldsymbol{U}$ is equal to unity:

$$\sum_{A \subseteq U} m(A) = 1 \tag{1}$$

The quantity $m(A)$ is the measure of the belief that is committed exactly to A but not to any particular subset of A. The belief in A is based on available evidence that supports exactly A. Because $m(A)$ is a measure of the belief committed exactly to A, it does not represent the total belief committed to A. In evidence theory, a measure of the total belief (degree of belief) in A is defined as

$$\mathrm{Bel}(A) = \sum_{B \subset A} m(B) \tag{2}$$

reflecting that the evidential support committed to one proposition is committed to any subset containing it. A subset A of $\boldsymbol{U}$ is called a focal element of a belief function Bel over $\boldsymbol{U}$ if $m(A)>0$. The union of all focal elements of a belief function is called its core. The plausibility measure is related to the basic probability assignment m:

$$\mathrm{Pl}(A) = \sum_{B \cap A \neq \varnothing} m(B) \tag{3}$$

Belief and plausibility measures are related by the equation $\mathrm{Pl}(A) = 1 - \mathrm{Bel}(\bar{A})$. Some properties of these measures are

$$\mathrm{Bel}(\varnothing) = \mathrm{Pl}(\varnothing) = 0, \qquad \mathrm{Bel}(\boldsymbol{U}) = \mathrm{Pl}(\boldsymbol{U}) = 1, \qquad \mathrm{Bel}(A) \le \mathrm{Pl}(A)$$

Also if $B \subseteq A$, then $\mathrm{Bel}(B) \le \mathrm{Bel}(A)$ and $\mathrm{Pl}(B) \le \mathrm{Pl}(A)$, and $\mathrm{Bel}(A) + \mathrm{Bel}(\bar{A}) \le 1$ and $\mathrm{Pl}(A) + \mathrm{Pl}(\bar{A}) \ge 1$. The last two expressions show that the two measures are nonadditive, that is, the sum of belief measures and the sum of plausibility measures are not required to be equal to unity. It is a consequence of uncertainty in available evidence. When evidence supports with certainty mutually exclusive propositions, the two measures coincide and the additivity rule is recovered.

Notice that the way one defines subsets A of $\boldsymbol{U}$ and links actual evidence to their basic assignments $m(A)$ depends on the problem being considered, one's current limited knowledge, and available evidence. Additional information can change the set of propositions and how evidence determines our degree of belief $\mathrm{Bel}(A)$ in these propositions.

Dempster's rule is a technique for combining evidence from different sources to improve predictions. Mathematically, application of Dempster's rule to two or more belief functions over the same set $\boldsymbol{U}$ yields a new belief function called their orthogonal sum. In the simplest case of two belief functions Bel_1 and Bel_2 with basic probability assignment functions m_1 and m_2, Dempster's rule provides the orthogonal sum:

$$m(C) = \sum_{\substack{i,j \\ A_i \cap B_j = C}} m_1(A_i) m_2(B_j) \Bigg/ \left[1 - \sum_{\substack{i,j \\ A_i \cap B_j = \varnothing}} m_1(A_i) m_2(B_j) \right] \tag{4}$$

where $C = A_i \cap B_j$ and $A_1, \ldots, A_k$ and $B_1, \ldots, B_k$ are focal elements of Bel_1 and Bel_2, respectively. The core of the belief function given by m is equal to the intersection of the cores of Bel_1 and Bel_2. The belief function $\mathrm{Bel}(C)$ resulting from the combination can then be obtained from m using Eq. (2).

For valid use of Dempster's rule, belief functions Bel_1 and Bel_2 must satisfy some conditions (Ref. 9): they should not strictly contradict each other and they should be based on independent sources of evidence. We discuss how to satisfy these requirements for the specific problem being considered in the paper in the following sections.

III. Problem Statement

We consider a turbulent flow around the Royal Aircraft Establishment (RAE) 2822, for which experimental results are available at the following operating conditions (case 1 of Ref. 17): freestream Mach number $M_\infty = 0.676$, angle of attack $\alpha = 2.4$, and Reynolds number (based on the freestream velocity and the airfoil chord) equal to 5.7×10^6. Computations of the relevant stationary turbulent flowfield are performed with the ISAAC code,[18] which is based on a second-order finite volume algorithm for solving the

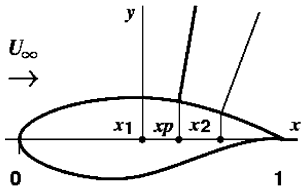

Fig. 1 Velocity profiles calculated at *x*1, *x*2, and *xp* positions; experimental data available only at *x*1 and *x*2.

Favre-averaged Navier–Stokes equations coupled with several turbulence models. In the present study, the standard k–ε (Ref. 19) and k–ω (Ref. 20) turbulence models are used. Details of the turbulence model equations and computational procedure may be found in Ref. 18. The grid is a nonuniform C mesh with 257 mesh points in the wraparound direction (with 177 points on the airfoil surface) and 97 points in the wall-normal direction. The grid extends approximately 18 chords from the airfoil. The same grid is used in all computations.

The problem is to quantify the uncertainty in the computed streamwise mean velocity profiles at prescribed chordwise positions, for example, $x1$ and $x2$ in Fig. 1, in the light of experimental data and to predict the velocity profile at a new location xp.

IV. Solution Procedure and Results

In this section, we explain how the basic concepts of evidence theory can be applied to quantify uncertainty. Specifically, uncertainty is quantified in terms of a basic probability assignment function (m function) for intervals in which the deviation of computed results from experimental data falls. These m functions are combined with the predictions of turbulence models at a new location (xp in Fig. 1), where experimental data are unavailable. The resultant predictions of these models are fused using Dempster's rule (at each ordinate along the normal to the airfoil surface) to determine 1) the intervals in which velocity value is likely to fall and 2) the measure of belief for each interval. This procedure is expected to yield a more reliable prediction of the velocity profile at this location than each turbulence model does separately.

A. Uncertainty Quantification in Turbulent Streamwise Velocity Profiles

We choose the deviation of the computed streamwise velocity profile from experimental data as the evidence to work with. The deviation (Dev) is defined as

$$\text{Dev} = (U_e - U_m)/U_\infty \tag{5}$$

Experimental data on turbulent flows are usually averaged flow quantities (not individual realizations). In the present instance, they are mean velocity profiles from Ref. 17. The deviation is computed at positions $(x/c,\ y/c)$ where experimental data are available (using interpolation, if necessary), and thus, it is a function of position.

As the experimental data available to calculate deviation values (Dev values) is finite, the range of deviation is finite as well. Therefore, it is always possible to specify at least a single finite interval, which includes all Dev values. Based on this observation, one can say that all available evidence (Dev values) supports the proposition that the deviation of mean velocity value (computed with a given turbulence model using given grid and numerical procedure) from corresponding experimental data is likely to fall inside this finite interval. Obviously, our proposition that evidence supports this specific interval is subjective and corresponds to the available database. More experimental data could possibly increase the size of this interval.

The single interval supported by evidence is not very informative. Different uncertainty sources can favor different ranges of Dev values. To study the distribution of Dev values (Dev distribution), the single interval is divided into subintervals of uniform size ΔDev, which we call the deviation step. (We assume the subintervals to be of uniform size for the sake of simplicity.) Each Dev value unambiguously supports one of the subintervals. If the available Dev values are few, or if ΔDev is small, the Dev distribution will be scattered: there may be no pronounced maximum, and unsupported subintervals (Dev intervals) may alternate with supported ones. A scattered deviation distribution yields no useful information. A deviation distribution over the single interval and one scattered over several subintervals are two limits of possible Dev distributions, which are not very informative. We observe that, for the purpose of the present work, the most useful Dev distribution would be one that is of the concave type, that is, with one subinterval with maximum evidence support (more Dev values fall inside this subinterval) and with the evidence to support subintervals on both sides of this subinterval monotonically decreasing. Subintervals with nonzero support are focal elements of the Dev distribution, and the set of all of them constitutes its core. Although there is no guarantee that for any engineering problem there exists such a ΔDev that allows one to construct the Dev distribution with the desirable property of a concave shape, interestingly enough it turned out to be the case in the problem considered in the present paper.

In the case of Dev values distributed over a set of subintervals instead of a single interval, we define the basic probability assignment for each subinterval as the ratio of the number n of Dev values falling inside the subinterval to the total number N of Dev values used to build the Dev distribution:

$$m(\Delta_i\text{Dev}) = n_i/N \tag{6}$$

where i is the index over focal elements of the Dev distribution. In this case, because all subintervals are disjoint and there is no ambiguity in how evidence supports different subintervals, the BPA for each subinterval is equal to the degree of belief and the degree of plausibility [see expressions (2) and (3)]:

$$m(\Delta_i\text{Dev}) = \text{Bel}(\Delta_i\text{Dev}) = \text{Pl}(\Delta_i\text{Dev}) \tag{7}$$

In deviation distributions constructed in such a manner, the subinterval with the maximum support shows how far the uncertainties and errors in the computational procedure (which includes model uncertainty, grid resolution, experimental error, etc.) will likely force the simulation results to deviate from reality (represented by experimental data). Obviously, the most favorable scenario would be the one where the most supported subinterval includes the zero Dev value. Another feature of a Dev distribution to be considered is the size of its core. The smaller this size, the more focused is the combined contribution of uncertainty sources and better is the accuracy of the simulation. The size of ΔDev indicates whether evidence supports one subinterval over others. The smaller ΔDev one can choose without compromising the properties of the Dev distribution, the better is the accuracy of predictions that can be achieved, as will be shown in the following sections.

These three characteristics, the location of the maximum, the size of ΔDev, and total range of Dev values, of Dev distributions can be used to compare, for instance, the accuracy of simulations with different turbulence models and the effectiveness of changes in computational procedure. However, these topics are beyond the scope of the present paper. The current paper focuses only on exploring the possibility of using the information provided by Dev distributions to quantify uncertainty and improve the accuracy of turbulent flow predictions in situations where no data representing reality are available.

Intuitively, the more experimental data used, the more confidence we have in a Dev distribution. For example, let us consider two Dev distributions, Dev_1 and Dev_2, that are constructed based on experimental data sets N_1 and N_2, respectively. Assume that $N_1 > N_2$. Then, BPAs for subintervals of the Dev_1 distribution calculated by expression (6) do not change. In other words, the total belief in the distribution built using the largest number of available data does not change. For the Dev_2 distribution, BPAs have to be recalculated though:

$$m(\Delta_i\text{Dev}_2) = n_i/N_1 \tag{8}$$

where i now is the index over subintervals with nonzero support of the Dev_2 distribution and

$$\sum_i n_i = N_2$$

The sum of BPAs determined by expression (8) is less than 1:

$$\sum_i m(\Delta_i \mathrm{Dev}) = \frac{N_2}{N_1} < 1$$

To satisfy condition (1), we assign the BPA equal to $(N_1 - N_2)/N_1$ not to any individual subinterval specifically, but to the set of all possible Dev values and call it uncommitted belief. It reflects that, if we had additional N_1–N_2 experimental data, we would not know which Dev subintervals they would support.

B. Application of Deviation Distributions for Predictions

In this section, we describe a procedure we developed to quantify and, possibly, improve predictions of turbulent flows, that is, simulation of a flow for which no reference data, such as experimental or results of direct numerical simulations, are available. The procedure relies on the results of computations with turbulence models and Dev distributions used to assess the accuracy of simulations made with these models in a controlled environment. In the procedure, we do not choose between various turbulence models. Instead, we fuse the information they provide.

Mean velocity values calculated by two turbulence models, k–ε (Ref. 19) and k–ω (Ref. 20), are known at any mesh point or can be interpolated to any flow position of interest. Experimental data are available only at a few positions along the airfoil chord in the y direction normal to the airfoil surface. For instance, in the flow over the upper surface of the airfoil, there are 20 experimental mean velocity values along the y direction at $x/c = 0.75$ and 28 values at $x/c = 0.95$ (in accordance with Ref. 17). Let us assume that there are no experimental data at $x/c = 0.9$, but we would like to predict $U(y/c)$ at this position and to determine the accuracy of the prediction (Fig. 1, $xp = 0.9$). The procedure includes six steps:

1) Dev distributions are built for both models at each position: $x/c = 0.75$ ($x1$ in Fig. 1) and $x/c = 0.95$ ($x2$ in Fig. 1). Four Dev distributions and four m functions attributed to these Dev distributions result from this step.

2) The m functions from step 1 are independently applied at each mesh point in the y direction to velocity profiles calculated at $x/c = 0.9$. For each model, one obtains two different, but equally likely, sets of supported intervals around a computed $U(y/c)$. Different sets correspond to the m functions obtained at different x/c positions. Each set reflects our belief that the true value of $U(y/c)$ lies inside of one of its intervals and that BPAs of different intervals define the degree of belief that we associate with each interval.

3) Dempster's rule is applied to combine at each y/c position the sets of intervals of possible true velocity values obtained for different turbulence models using the m functions from different x/c positions. Two different, but equally likely, solutions are obtained.

4) The two solutions are averaged to produce a single set of intervals of possible true velocity values at each y/c.

5) To eliminate possible discontinuities introduced by steps 3 and 4 in velocity values at adjacent y/c positions, a smoothing procedure is applied to the solution obtained in step 4.

6) At each y/c position, the interval with maximum degree of belief is extracted. Such intervals form a velocity profile along the y direction, which we call the swath of maximum degree of belief. The swath of maximum degree of belief is supposed to be more reliable than individual turbulence model calculations and, ideally, coincides with experimental data, if they are available.

In sum, evidence theory tools are applied in steps 1 and 3. Next, techniques for all steps are described in detail. Although the procedure is described for two statistical turbulence models, there are no limitations on the number of turbulence models, the type of models, and the kind of flow this procedure can be applied to. For instance, results from statistical turbulence models can be fused with those of large-eddy simulations or with the data produced by any other method. Also, there is no restriction on the location of specific x/c positions.

Step 1

Because we use Dempster's rule to fuse information from different sources (results of simulations with different turbulence models), it is required that the degrees of belief to be combined should be based on independent sources of evidence. Independence of evidence sources is important, but its definition is highly subjective.[15] Because we are working with Dev distributions, it stands to reason to assume that the Dev distributions are independent of one another if they are constructed using the results of calculations based on different turbulence models and different experimental data. In the current study, it means that we have to build a Dev distribution related to the k–ε model at one x/c position, for example, $x/c = 0.75$, and a Dev distribution related to the k–ω model at different x/c position, for example, $x/c = 0.95$, or vice versa. Thus, in this step, we build two Dev distributions (at $x/c = 0.75$ and $x/c = 0.95$) for each turbulence model.

In Sec. IV.A we provide the details on the construction of Dev distributions. We note, however, that 20 (or 28) points turned out to be insufficient to build informative Dev distributions with a concave shape. Therefore, we build distributions of not exactly Dev values defined by expression (5), but of their absolute values. This is not a requirement of the procedure in any way, but solely due to limited data available at given x/c positions in this flow. By ignoring the sign of deviations, we increase the amount of Dev values falling inside each subinterval. Note that, although limited experimental data appear to be a disadvantage for testing the approach, in fact, quite the opposite is true. If an approach works in the worst conditions, then this is definitely an advantage of the approach. This also shows that this specific type of uncertainty (Dev sign) is not of prime importance, at least in the present instance.

Four Dev distributions are used to determine m functions associated with each of them. One has to take into account that to build Dev distributions at $x/c = 0.75$ only 20 experimental values are used. At $x/c = 0.95$, there are 28 values available. Thus, expression (6) is used to calculate BPAs for subintervals of Dev distributions obtained at $x/c = 0.95$, and expression (8) is used to calculate BPAs for individual subintervals of Dev distributions obtained at $x/c = 0.75$. A BPA equal to 8/28 is assigned as the uncommitted belief to each Dev distribution obtained at $x/c = 0.75$. BPAs committed to individual subintervals of all four Dev distributions are shown in Fig. 2. Uncommitted belief is not shown in Fig. 2a or 2b.

Step 2

Expression (5) can be used for prediction in the following manner. If one knows the value of the deviation and the calculated value, one can try to define the "true" velocity value, that is, the value, that would coincide with the experimental data if available. There is no guarantee, but it is our belief that the velocity value found in such a way would better reflect reality. Thus, we rewrite expression (5) in the following way:

$$U_p/U_\infty = U_m/U_\infty + \mathrm{Dev} \tag{9}$$

We do not know the Dev value, but we do know the Dev distributions built in step 1 that provide information about which Dev subintervals have nonzero BPA. Thus, instead of one velocity value, which would be given by expression (9), we have information on how different velocity intervals would be supported by evidence, which in this case is given by BPAs for Dev subintervals determined in step 1. If U_m is the mean velocity value calculated by, for instance, the k–ε model at a given y/c position at $x/c = 0.9$, and $\Delta_i \mathrm{Dev}$ are subintervals of the Dev distribution for this model built at $x/c = 0.95$, then we determine the supported velocity intervals as

$$\Delta_i U_p/U_\infty = U_m/U_\infty + \Delta_i \mathrm{Dev} \tag{10}$$

given that the y/c positions are those of mesh points. Recall that the Dev distributions, in contrast to velocity values at a given x/c

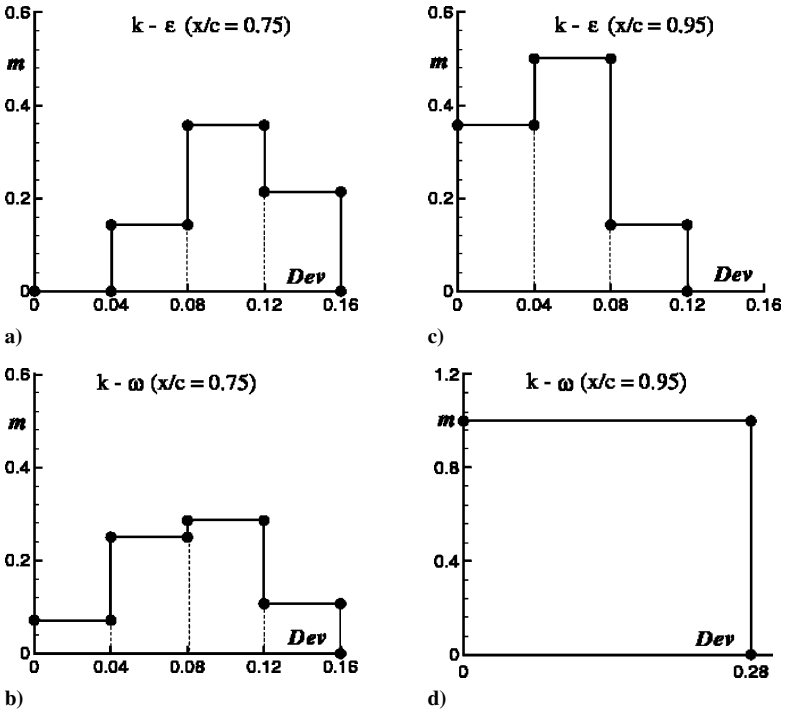

Fig. 2 BPAs for individual intervals of Dev distributions obtained in step 1.

position, are not dependent on y/c, and thus, the same Dev distribution is added to different values of U_m along the y direction. BPAs of Dev subintervals are directly reassigned to corresponding velocity intervals as

$$m(\Delta_i U_p/U_\infty) = m(\Delta_i \text{Dev}) \tag{11}$$

This procedure explains why the single maximum is a desirable property of a Dev distribution. In a given flow at a given flow position $(x/c, y/c)$, there could be only one velocity value and one velocity interval that includes this value. Thus, evidence should favor one interval over others to avoid contradiction.

Because we ignore the sign of deviation in the present case to increase statistics, we do not know on which side of the calculated velocity value lies the true velocity value; we apply to the calculated velocity value the same Dev intervals symmetrically on both sides of U_m. Velocity intervals on the right side $(\Delta_i U_p^r)$ and left side $(\Delta_i U_p^l)$ of U_m are found as

$$\Delta_i U_p^r \big/ U_\infty = U_m/U_\infty + \Delta_i\,|\text{Dev}|$$

$$\Delta_i U_p^l \big/ U_\infty = U_m/U_\infty - \Delta_i\,|\text{Dev}|$$

Basic probability assignment functions are also applied to the velocity intervals symmetrically about U_m:

$$m\left(\Delta_i U_P^r \big/ U_\infty\right) = m(\Delta_i \text{Dev}), \qquad m\left(\Delta_i U_P^l \big/ U_\infty\right) = m^*(\Delta_i \text{Dev})$$

where m^* is the mirror reflection of m. The uncommitted belief assigned to Dev distributions at $x/c = 0.75$ is assigned to velocity intervals on either side of U_m. An example of how the m function for a Dev distribution transforms into BPAs for individual velocity intervals around $U_m(y/c)$ at $x/c = 0.9$ is shown in Fig. 3. BPAs in Fig. 3 are obtained from the BPAs shown in Fig. 2a. Figure 4 shows the result of application of the BPAs from Fig. 3 to the velocity profile calculated with the k–ε model (black solid line) at $x/c = 0.9$. The true velocity profile is expected to occur inside the band of colors. Different colors correspond to different degrees of belief assigned to different areas inside the band.

Because there are twice as many supported velocity intervals as original Dev subintervals, $\Delta_j U_p = (\Delta_i U_p^r, \Delta_i U_p^l)$, where j is the index over velocity intervals, and the same BPA is committed to

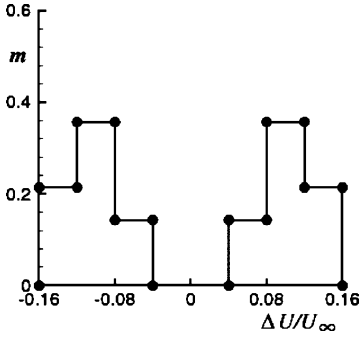

Fig. 3 BPAs obtained from Fig. 2a for individual velocity intervals around U_m at $x/c = 0.9$.

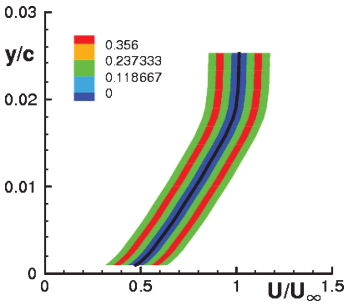

Fig. 4 Area of possible true velocity profile built around k–ε model profile (black line) at $x/c = 0.9$ using BPAs from Fig. 3: colors show BPAs of different areas.

each of velocity interval as to the corresponding Dev subinterval, it follows that

$$\sum_j m(\Delta_j U_p) = 2$$

in contradiction with expression (1). To resolve this issue, we simply lessen the BPA of each interval, as well as the amount of uncommitted belief by a factor of one-half.

Because one can apply two m functions (one from $x/c = 0.75$ and another from $x/c = 0.95$) to the single velocity profile calculated with each turbulence model at $x/c = 0.9$, one obtains two areas (bands similar to those shown in Fig. 4) where the true velocity profile could fall. We consider them as equally likely solutions.

To simplify the discussion, let us introduce notations for each solution. The area obtained by combining together the m function

obtained for the k–ε model at $x/c = 0.75$ and the velocity profile $U_m(y/c)$ calculated with the k–ε model at $x/c = 0.9$ is denoted as KE1. When the velocity profile $U_m(y/c)$ calculated with the k–ε model at $x/c = 0.9$ is combined with the m function specified for this model at $x/c = 0.95$, the solution is called KE2. Similarly, the two areas for the k–ω model are denoted as KW1 and KW2.

Step 3

In this step, we fuse areas of possible true velocity profile produced by different models, that is, we fuse KE1 and KW2 solutions, and independently, KE2 and KW1 solutions. By combining solutions in such a way, we satisfy the requirement of Dempster's rule for independence of evidence sources. (For more detail, see the discussion of step 1.) Fusing means that we apply Dempster's rule independently at each mesh point along the y direction at $x/c = 0.9$ to BPAs of velocity intervals specified for each turbulence model at a given y/c. Another requirement of Dempster's rule is that evidence from different sources should not strictly contradict each other. This requirement is implicitly satisfied in this problem: Areas of possible true velocity profile corresponding to different turbulence models overlap at any y/c. In problems where supported areas do not overlap, other fusing techniques should be considered instead of Dempster's rule.

First, we show how Dempster's rule works in a simple case. Let us assume that, at a given y/c position, the KE1 area consists only of the single interval ΔU_{KE1} with the BPA $m_1(\Delta U_{\mathrm{KE1}}) = s_1$ and with the rest of belief assigned to the set of all possible velocity values $m_1(\boldsymbol{U}) = 1 - s_1$ (uncommitted belief). At the same y/c position, the KW2 area also consists of one interval ΔU_{KW2} with the BPA $m_2(\Delta U_{\mathrm{KW2}}) = s_2$ and with the uncommitted belief $m_2(\boldsymbol{U}) = 1 - s_2$. The result of fusing two basic probability assignment functions, m_1 and m_2, can be presented as a table and is shown in Fig. 5. The entire table represents our total belief. Vertical strips are associated with BPAs of velocity intervals from the KE1 area and horizontal strips are associated with BPAs of velocity intervals from the KW2 area. The intersection of these two strips has measure, $m_1(\Delta_i U) \cdot m_2(\Delta_j U)$, where i and j are indices over intervals of functions m_1 and m_2, respectively. In our case, $i = j = 1$. The BPA of the intersection of two intervals is

$$m(\Delta U_{\mathrm{KE1}} \cap \Delta U_{\mathrm{KW2}} \neq \varnothing) = m_1(\Delta U_{\mathrm{KE1}}) \cdot m_2(\Delta U_{\mathrm{KW2}})$$

If each function, m_1 and m_2, assigns nonzero BPAs for several intervals, then an interval of m_1 can intersect with more than one interval of m_2. In this case, the BPA of the interval is the sum of measures of all related intersections. As Fig. 5 demonstrates, the uncommitted belief $m_2(\boldsymbol{U})$ contributes to the BPA of the ΔU_{KE1} interval, and in a similar manner, the uncommitted belief $m_1(\boldsymbol{U})$ contributes to the BPA of ΔU_{KW2} interval. The product of uncommitted beliefs does not relate to any specific interval. If two intervals do not intersect, the measure

$$m(\Delta U_{\mathrm{KE1}} \cap \Delta U_{\mathrm{KW2}} = \varnothing) = m_1(\Delta U_{\mathrm{KE1}}) \cdot m_2(\Delta U_{\mathrm{KW2}})$$

should be deduced from the total belief. Then, the BPAs for intersecting intervals should be renormalized accordingly. This is how expression (4) for Dempster's rule is derived.

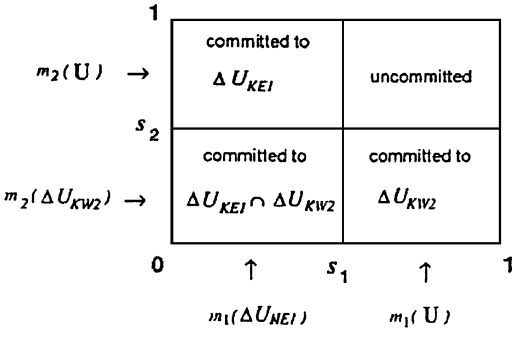

Fig. 5 Example of Dempster's rule application.

No area in Fig. 5 should be deduced from the total belief. Thus, renormalization is not required. Therefore, the basic probability assignment function m, which corresponds to Fig. 5, is defined as

$$m(\Delta U_{\mathrm{fus}}) = \begin{cases} s_1 \cdot s_2, & \text{if } \Delta U_{\mathrm{fus}} = \Delta U_{\mathrm{KE1}} \cap \Delta U_{\mathrm{KW2}} \\ s_1 \cdot (1 - s_2), & \text{if } \Delta U_{\mathrm{fus}} = \Delta U_{\mathrm{KE1}} \\ s_2 \cdot (1 - s_1), & \text{if } \Delta U_{\mathrm{fus}} = \Delta U_{\mathrm{KW2}} \\ (1 - s_1)(1 - s_2), & \text{if } \Delta U_{\mathrm{fus}} = \boldsymbol{U} \\ 0, & \text{if } \Delta U_{\mathrm{fus}} \text{ is any other interval} \\ & \quad \text{and } \Delta U_{\mathrm{fus}} < \boldsymbol{U} \end{cases} \tag{12}$$

The corresponding Bel function can be obtained from expression (2); plausibility functions are not used in the current study.

It is easy to see that fusing even the simplest m functions (defined over a single interval) results in a complex m function defined over several intervals of different size. Keeping in mind that 1) m functions, as those built in the preceding steps, include several intervals and 2) intervals of two functions intersect in different ways at different y/c positions, we decided to coarsen the set of intervals after fusing to avoid unnecessary complexity. The coarsening means that we calculate BPAs only for the set of intervals associated with one of the m functions used in fusing. This set has a minimum deviation step ΔDev. For instance, considering KE1 and KW2 solutions, we choose KE1 intervals (Figs. 2a and 2d). If the deviation steps of two m functions are of the same size, we choose the set of intervals with the highest degree of belief. BPAs for the chosen set are obtained by Dempster's rule [expression (4)]. Because the intervals of this set are disjoint, the total belief that the true velocity value is contained in an interval is equal to the BPA of that interval.

Fusing solutions KE1 and KW2 results in their combined solution R1 (Fig. 6a). Solution R2 is the result of combining KE2 and KW1 (Fig. 6b). The bands of color in Fig. 6 indicate the areas where the true velocity profile could fall. It is not expected that the true velocity profile will be found outside of these bands. Statistically, solutions R1 and R2 are equally likely. Therefore, they will be averaged in step 4.

Step 4

In this step, the two solutions R1 and R2 are averaged. The velocity intervals of the two solutions are combined at each y/c position independently. To resolve the mismatches in size and location of the velocity intervals of the two solutions, we choose the most refined

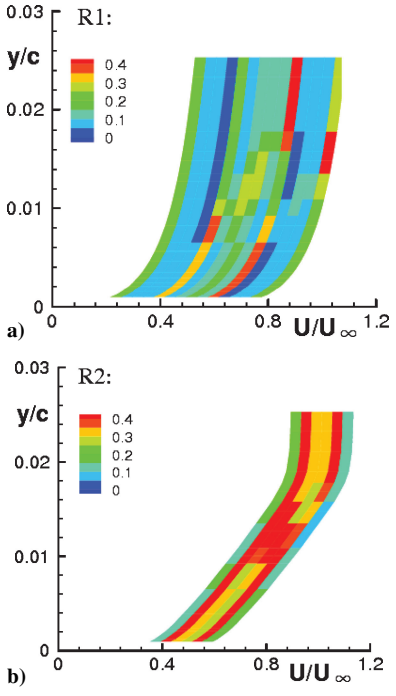

Fig. 6 Two equally likely velocity areas obtained in step 3.

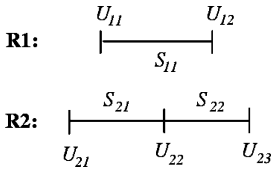

Fig. 7 Intersecting intervals of two solutions.

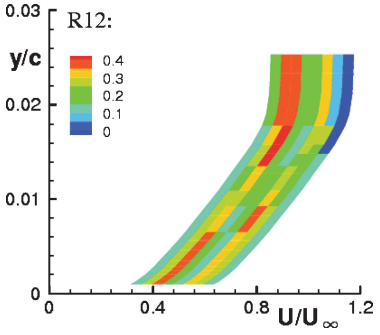

Fig. 8 Averaged solution.

interval set (with a minimum ΔDev) to increase the accuracy of predictions. Then, the other solution is projected onto the chosen set. The procedure is described next in detail.

Let us assume that the set of the R1 solution is more refined, and therefore, we will project the solution R2 onto the velocity intervals of the solution R1. At a given y/c, assignment m_{11} is the BPA of the velocity interval $[U_{11}, U_{12}]$ of the solution R1; m_{21} is the BPA of the velocity interval $[U_{21}, U_{22}]$ and m_{22} is the BPA of the velocity interval $[U_{22}, U_{23}]$ of the solution R2. The interval $[U_{11}, U_{12}]$ intersects both intervals of the solution R2 as shown in Fig. 7. Then, the BPA of the interval $[U_{11}, U_{12}]$ for the averaged solution is calculated by the formula

$$m = \tfrac{1}{3}\{m_{11} + m_{21}[(U_{22} - U_{11})/(U_{22} - U_{21})] + m_{22}[(U_{12} - U_{22})/(U_{23} - U_{22})]\}$$

which takes into account m_{21} and m_{22} with appropriate weights. Weights are determined by the fraction of an interval that overlaps with $[U_{11}, U_{12}]$. For other types of interval overlapping, a similar approach for calculating the averaged interval BPA should be applied. Figure 8 shows the result (R12) of averaging R1 and R2.

The averaging technique used in this paper is one of the simplest and is well suited to the present study.

Step 5

Initially, bypass this step and go to step 6. If the final velocity profile obtained in step 6 has discontinuities, perform step 5. An example of a solution with a discontinuity is shown in Fig. 9a. This velocity profile is extracted directly from the solution R12 (Fig. 8). Step 5 attempts to resolve this issue.

Any combination rule applied in such a way that the value at y/c is independent of the neighboring ones will likely lead to discontinuities in the solution. Also, using the absolute value of the deviation instead of the deviation itself leads to possible ambiguity in the position of the true velocity value at each y/c. The suggested smoothing procedure reestablishes the continuity of the mean velocity profile.

The procedure we use for smoothing is, in fact, a mathematical representation of a basic rule that exists in nature and society: the distributive property of a system of interacting elements. Obviously, different systems distribute a quantity in different ways. We are interested in the simplest and fastest procedure to redistribute our degrees of belief to take into account the interaction existing between velocity values at different y/c positions.

The system of interacting elements can be represented as a matrix, with matrix elements representing the system elements. The value of an element is equal to the amount of the quantity of interest that the element possesses initially. The degree of interaction between matrix elements is determined by their positions in the matrix. In relation to the problem considered in the paper, matrix elements are velocity intervals. Each row represents velocity intervals at the

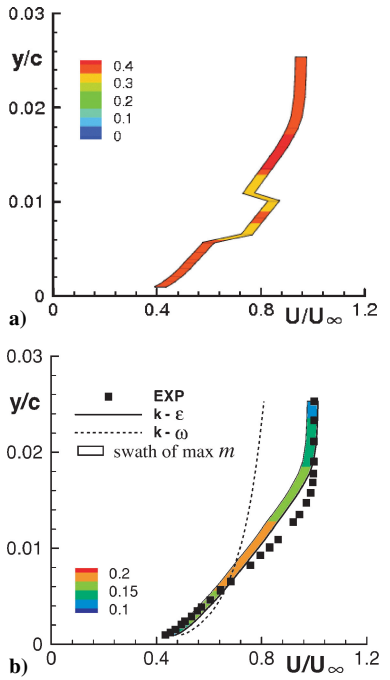

Fig. 9 Swath of maximum degree of belief: a) before smoothing and b) after smoothing.

same y/c position. The value of each matrix element is equal to the degree of belief it is assigned initially in the solution R12. In other words, the matrix constructed in such a manner is a mathematical representation of Fig. 8.

It is better to illustrate the smoothing procedure in application to a very simple case. Let us assume that we have a 3×3 matrix $\boldsymbol{A}$ with elements a_{ij}. Using an algorithm involving the distance between elements in matrix $\boldsymbol{A}$, we construct the new matrix $\boldsymbol{B}$ with elements b_{ij}:

$$b_{ij} = \sum_{k,l=1,\ldots,3} \frac{a_{kl}}{(|a_{ij} - a_{kj}| + 1)(|a_{ij} - a_{il}| + 1)} \tag{13}$$

In expression (13), the distance between matrix elements is defined as $|a_{ij+1} - a_{ij}| = |a_{i+1j} - a_{ij}| = 1$. In matrix $\boldsymbol{B}$, let element b_{22} be the largest. This value is used to normalize matrix $\boldsymbol{B}$ in such a way that element b_{22} would be equal to a_{22}. The new, normalized matrix (matrix $\boldsymbol{C}$) with elements

$$c_{ij} = a_{22} \cdot b_{ij}/b_{22} \tag{14}$$

is the smoothed one. The transformation of matrix $\boldsymbol{A}$ to matrix $\boldsymbol{C}$ is as follows for a simple example consisting of unit elements $a_{ij} = 1$:

$$\boldsymbol{A} = \begin{pmatrix} 1 & 1 & 1 \\ 1 & 1 & 1 \\ 1 & 1 & 1 \end{pmatrix} \qquad \boldsymbol{B} = \begin{pmatrix} 121/36 & 11/3 & 121/36 \\ 11/3 & 4 & 11/3 \\ 121/36 & 11/3 & 121/36 \end{pmatrix}$$

$$\boldsymbol{C} = \begin{pmatrix} 121/144 & 11/12 & 121/144 \\ 11/12 & 1 & 11/12 \\ 121/144 & 11/12 & 121/144 \end{pmatrix}$$

The matrix $\boldsymbol{A}$ constructed for the solution R12 (Fig. 8) consists of 27×8 elements (27 elements along the y direction and 8 velocity intervals at each y/c). A smoothed distribution of belief over the entire velocity area is obtained in two iterations.

Obviously, the degree of belief that the resultant matrix $\boldsymbol{C}$ assigns to its elements depends significantly on the smoothing algorithm used to construct the matrix $\boldsymbol{B}$. In this sense, the algorithm we just described is not unique. Other problems might require modifications of expression (13) or the development of other approaches. However,

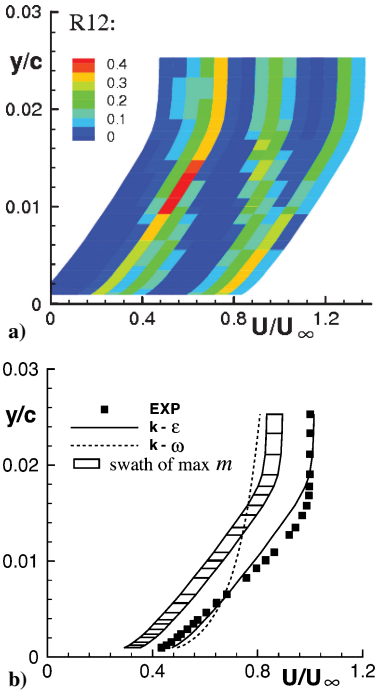

Fig. 10 Solution R12 a) obtained at x/c = 0.9 with m functions from x/c = 0.95 and x/c = 0.319 and b) swath of maximum support extracted from this solution.

for the problem considered in this paper, the algorithm has worked well.

Step 6

At each position y/c, one can select the single interval that has the highest belief that the true velocity value lies inside that interval. When such intervals are connected along the y direction, the swath of maximum degree of belief can be extracted. This swath is the most probable candidate to include the true velocity profile. In Fig. 9a, such a swath is shown for the solution R12 before it is smoothed. For smoothed solution R12 (not shown here), the swath of maximum degree of belief is given in Fig. 9b.

The swath from Fig. 9b is the final prediction of the approach considered in this study. In Fig. 9b, the swath is compared with the velocity profiles calculated by the k–ω model (dashed line) and by the k–ε model (solid line). Also, experimental data (black squares) are shown in Fig. 9b to assess the quality of the prediction. One can see that the k–ω model result is far from the experimental values, whereas the k–ε model is in very good agreement with the experiment. Our approach combines the results of both models, and yet, our prediction is also in very good agreement with the experiment. It shows a good potential of the approach to correctly weight contributions from different sources. Also, in contrast to the k–ε model result, our approach produces not just a single line, the accuracy of which cannot be estimated in the absence of experimental data, but zones with well-defined degrees of belief. This is an obvious advantage of the present method.

C. Influence of Other Sources of Uncertainty on the Solution

In the example considered, we did not take into account that the first x/c position ($x/c = 0.75$), where we built Dev distributions, lies farther from the x/c position ($x/c = 0.9$), at which we make the prediction, than the second x/c position ($x/c = 0.95$). In the future, it would be interesting to explore how to quantify this type of uncertainty. In the current study, we have only studied how the lack of such information influences the predictions.

For the case considered, it turns out that the prediction is not influenced by neglecting this source of uncertainty. However, what will happen if a validation point is far from the prediction point? In the next example, we try to answer this question by shifting one validation point to the position $x/c = 0.319$. The other validation point and the prediction point are at the same positions as in the earlier example, $x/c = 0.95$ and 0.9, respectively.

For this case, only the averaged R12 solution (Fig. 10a) and the smooth swath of maximum degree of belief (Fig. 10b) are shown. To obtain the smooth swath, three iterations are made in step 5. One can see that degrees of belief of velocity intervals are lost during smoothing in this case. The reason is that after the smoothing the maximum element in matrix $\boldsymbol{B}$ corresponds to the zero-value element in the initial matrix $\boldsymbol{A}$. Therefore, the calculation of elements in the matrix $\boldsymbol{C}$ by expression (14) returns zero. One can consider such a result either a shortcoming of the smoothing procedure or a clear indicator that, in this case, the uncertainty resulting from different distances between x/c positions does influence the result of the prediction and, therefore, should be explicitly included in the procedure. This issue will be addressed in future studies.

The prediction quality itself is also worse than in the preceding case. Still, even in such an unfavorable situation, the position of the true velocity profile predicted by the approach is qualitatively more correct than the profile calculated by the k–ω model. Thus, it allows us to infer that, in the absence of experimental data, the suggested approach is more reliable than the result of a single model calculation, even though not all sources of uncertainty are taken into account. In addition, we note that the approach is flexible enough to incorporate uncertainty from various sources to improve prediction quality.

V. Conclusions

An approach for quantifying uncertainty in turbulent flow simulations and for using this information to quantify and improve the quality of predictions in untested conditions is developed. The approach relies on the mathematical tools of evidence theory, which are customized here for application to total uncertainty in simulations.

Application of this approach to a subsonic turbulent flow around the RAE 2822 airfoil has provided encouraging results. In the future, we plan to apply the approach to other cases of the RAE 2822 flow, introduce a mathematical description of uncertainty originating from the distance between validation and prediction points, and consider the prediction of other flow parameters, as well as predict flow around an airfoil using results of validation of turbulence models in flows around other types of airfoils.

Note that this approach is not restricted to turbulent flows, or even, more generally, to aerodynamic flows. We believe that any problem that involves different modeling alternatives and has appropriate data can benefit from this approach.

Acknowledgments

This research was partially supported through NASA Ames Research Center Cooperative Agreement NCC2-1349. Also, the authors are thankful to T. A. Zang (NASA Langley Research Center) and W. Oberkampf (Sandia National Laboratories) for bringing to our attention valuable references. It is pleasure to acknowledge the comments of reviewers, which helped enhance the clarity of presentation.

References

[1]*Guide for the Verification and Validation of Computational Fluid Dynamics Simulations*, AIAA-G-077-1998, AIAA, Reston, VA, 1998.

[2]Casey, M., and Wintergerste, T. (eds.), *Best Practice Guidelines*, ERCOFTAC Special Interest Group on Quality and Trust in Industrial CFD, European Research Community on Flow, Turbulence and Combustion, 2000.

[3]Oberkampf, W. L., and Blottner, F. G., "Issues in Computational Fluid Dynamics Code Verification and Validation," *AIAA Journal*, Vol. 36, No. 5, 1998, pp. 687–695.

[4]Luckring, J. M., Hemsch, M. J., and Morrison, J. H., "Uncertainty in Computational Aerodynamics," AIAA Paper 2003-0409, Jan. 2003.

[5]Oberkampf, W. L., Trucano, T. G., and Hirsch, C., "Verification, Validation, and Predictive Capability in Computational Engineering and Physics," *Applied Mechanics Review*, Vol. 57, No. 5, 2004, pp. 345–384.

[6]Klir, G. J., and Wierman, M. J., *Uncertainty-Based Information: Elements of Generalized Information Theory*, Physica-Verlag, Heidelberg, Germany, 1998.

[7]Dubois, D., and Prade, H., *Possibility Theory: an Approach to Computerized Processing of Uncertainty*, Plenum, New York, 1988.

[8]Helton, J. C., and Oberkampf, W. L. (eds.), "Alternative Representation of Epistemic Uncertainty," *Reliability Engineering and System Safety*, Special Issue, Vol. 85, 2004.

[9]Shafer, G., *A Mathematical Theory of Evidence*, Princeton Univ. Press, Princeton, NJ, 1976.

[10]Oberkampf, W. L., Helton, J. C., and Sentz, K., "Mathematical Representation of Uncertainty," AIAA Paper 2001-1645, April 2001.

[11]Zadeh, L. A., "A Mathematical Theory of Evidence," *AI Magazine*, Vol. 5, No. 3, 1984, pp. 81–83.

[12]Shafer, G., "Belief Functions and Possibility Measures," *The Analysis of Fuzzy Information*, edited by J. C. Bezdek, Vol. 1, CRC Press, Boca Raton, FL, 1987, pp. 51–84.

[13]Sentz, K., and Ferson, S., "Combination of Evidence in Dempster-Shafer Theory," Sandia National Labs., Rept. SAND2002-0835, 2002.

[14]Yager, R. R., Kacprzyk, J., and Fedrizzi, M. (eds.), *Advances in the Dempster-Shafer Theory of Evidence*, Wiley, New York, 1994.

[15]Shafer, G., "Perspectives on the Theory and Practice of Belief Functions," *International Journal of Approximate Reasoning*, Vol. 4, No. 5–6, 1990, pp. 323–362.

[16]Shafer, G., "A Theory of Statistical Evidence," *Foundations of Probability Theory, Statistical Inference, and Statistical Theories of Science*, edited by W. L. Harper and C. A. Hooker, Vol. 2, D. Reidel, Boston, 1976, pp. 365–436.

[17]"Experimental Data Base for Computer Program Assessment," AGARD AR-138, May 1979.

[18]Morrison, J. H., "A Comprehensive Navier–Stokes Solver with Two-Equation and Reynolds-Stress Turbulence Closure Models," NASA CR 4440, May 1992; see also http://isaac-cfd.sourceforge.net/.

[19]Speziale, C. G., Abid, R., and Anderson, E. C., "Critical Evaluation of Two-Equation Models for Near-Wall Turbulence," *AIAA Journal*, Vol. 30, No. 2, 1993, pp. 324–331.

[20]Wilcox, D. C., *Turbulence Modeling for CFD*, DCW Industries, La Cañada, CA, 1993.

P. Givi
Associate Editor